FG03-95ER61986

Spectral Signature of Column Solar Radiation Absorption During the Atmospheric Radiation Measurement Enhanced Shortwave Experiment (ARESE)

William O'Hirok[1], Catherine Gautier[1,2], and Paul Ricchiazzi[1]

(1) Institute for Computational Earth System Science and

(2) Department of Geography

University of California Santa Barbara, CA

Revision

November 1999

Submitted to Journal of Geophysical Research - Atmosphere

DISCLAIMER

DISCLAIMER

Portions of this document may be illegible in electronic image products. Images are produced from the best available original document.

Abstract

Spectral and broadband shortwave radiative flux data obtained from the Atmospheric Radiation Measurement Enhanced Shortwave Experiment (ARESE) are compared with 3-D radiative transfer computations for the cloud field of October 30, 1995. Because the absorption of broadband solar radiation in the cloudy atmosphere deduced from observations and modeled differ by 135 Wm^{-2}, we performed a consistency analysis using spectral observations and the model to integrate for wavelengths between the spectral observations. To match spectral measurements, aerosols need a reduction in both single scattering albedo (from 0.938 to 0.82) and asymmetry factor (from 0.67 to 0.61), and cloud droplets require a three-fold increase in co-albedo. Even after modifying the model inputs and microphysics the difference in total broadband absorption is still of the order of $75Wm^{-2}$. Finally, an unexplained absorber centered around 1.06 μm appears in the comparison that is much too large to be explained by dimers.

1. Introduction

The absorption of solar radiation in the atmosphere has been a considerably debated issue for more than four decades. For many years, the focus was on understanding and explaining the discrepancy between aircraft observations and theoretical estimates of solar radiation absorption and reflectance by clouds (e.g., Stephens and Tsay, 1990). A new version of the debate was initiated a few years ago following comparisons between satellite observations and climate model computations of the absorption of solar radiation in cloudy skies. Essentially, the contention is that while in climate models the absorption of solar radiation in cloudy and clear atmospheres is equivalent, observations suggest much greater absorption in a cloudy atmospheric column. This discrepancy is a crucial issue for climate model predictions, since the amount of solar radiation absorbed by the atmosphere strongly influences exchanges of heat between atmosphere and ocean and their dynamics.

Following the advent of Earth radiation measurements from space (Ramanathan, 1987), a high degree of confidence now exists on the total solar radiation absorbed by the Earth system (combined atmosphere and surface) for clear or cloudy conditions. However, the determination alone of the solar radiation absorbed by the atmosphere requires the differential measurement of the observed net fluxes between both the top of the atmosphere and surface. This measurement is, itself, fraught with uncertainties. There are two extreme positions from which one can speculate about the discrepancy between observations and models: the difference is produced by observational or analysis uncertainties or the discrepancy is the result of climate model inadequacies. Most likely, the solution lies somewhere in between these two competing explanations.

Over the last few years, many papers have appeared that deal with the topic of excess observed absorption (referenced to model computations), also commonly referred to as anomalous absorption (Ramanathan et al. 1995, Cess et al., 1995, 1996, Pilewskie and Valero, 1995, Waliser et al., 1996 and Collins, 1998). These papers have shown the existence of excess absorption (15 – 35 Wm^{-2} diurnal average) that is both too large to be attributed to standard observational error and cannot be explained by existing radiative transfer theory. Their evidence is based on surface or low-flying aircraft observations coupled with top of the atmosphere observations from aircraft or satellites. However, using similar approaches Li and Moreau (1995) and Imre et al. (1996) among others suggest that anomalous absorption is negligible or

at most limited to the Tropics. Although many physical mechanisms have been suggested to explain anomalous absorption (Stephens and Tsay, 1990) none have been clearly able to account for its magnitude for all observed conditions.

In order to decisively answer the claim of anomalous absorption, the Atmospheric Radiation Measurement Enhanced Shortwave Experiment (ARESE) was conducted by the Department of Energy in fall, 1995. ARESE consisted of many different surface, aircraft, and satellite observations. Based on a set of coordinated aircraft observations, recent papers (Zender et al.,1997, Valero et al., 1997a, Valero et al., 1997b) have supported the existence of anomalous absorption in cloudy sky conditions with computed magnitudes of nearly $100 Wm^{-2}$ for the flight of October 30, 1995. This most recent demonstration (Zender et al., 1997) is based on a set of broadband measurements. However, Li et al. (1999) using a variety of observations from more sources including aircraft, spacecraft and ground-based instruments suggest that the anomaly may be related to the "quality" of the total solar broadband radiometer data.

In this study, we check the consistency of the broadband observations with spectral measurements taken during the ARESE experiment to evaluate whether uncertainties in these observations could be the source of the anomaly. Toward that end we employed a 3-D spectrally resolved radiative transfer model developed to simulate the 3-D radiation field in a cloudy atmosphere (O'Hirok and Gautier, 1998a). Although we anticipated minimal 3-D absorptive effects with the type of clouds present on the day analyzed, the 3-D model was used to provide a realistic smooth upwelling radiation field that cannot be directly obtained from standard 1-D models.

Here we present observations and model computations for a 3-D representation of the thick stratus cloud system that occurred during ARESE on October 30 1995 (103095). Consistency amongst different sets of observations is analyzed and discussed, and modifications to physical processes are provided to demonstrate how the gap between the observations and theory can be reduced.

2 Method

2.1 Observations

Radiometric measurements were obtained from the Grob Egrett aircraft flying over the cloud layer at approximately 13 km above ground level (agl) and the Twin Otter aircraft located beneath the cloud at a

mean altitude of 0.5 km agl. Two identical radiometric instrument packages of the Radiation Measurement System (RAMS) were outfitted on each aircraft (Valero et al., 1997b). Two types of broadband radiometric instruments and a spectrally resolved radiometer were deployed, each providing simultaneous observations in both the nadir and zenith direction. The Total Solar Broadband Radiometer (TSBR) encompasses the solar spectrum between 0.224 and 3.91 μm, and the Fractional Solar Broadband Radiometer covers the near-infrared between 0.68 and 3.3 μm. As calculated in Zender et al. (1997), the visible irradiance is defined as the difference between the TSBR and FSBR. The solar irradiance at seven spectral bands (approximately 10 nm wide) centered at 0.500, 0.862, 1.064, 1.249, 1.501, 1.651 and 1.750 μm were measured using the Total Direct Diffused Radiometer (TDDR). The absolute accuracy of the TSBR/FSBR is probably of the order of 2 – 3%, and that of the TDDR is 5 % (Valero et al., 1997b).

The TSBR/FSBR data sets used in this study have a release date of August 12, 1997 for the Egrett and August 22, 1997 for the Twin Otter. The TDDR data sets release dates are June 18, 1997 for the Egrett and June 9, 1997 for the Twin Otter. These data sets represent the latest refined calibration "b1" data sets and are the most currently available as of June 25, 1998 (Bush, 1998 personal communication).

TDDR fluxes used in the analysis of this paper have been converted from Wm^{-2} to $Wm^{-2}\mu m^{-1}$ by dividing by the spectral bandwidths contained within the TDDR data files. Additionally, model computations of TSBR and FSBR fluxes use the filter functions supplied with the TSBR/FSBR data sets. Nadir viewing spectral reflectance (0.418 - 1.096 μm) from the Egrett was also obtained from observations made by the Scanning Spectral Polarimeter (SSP). The SSP has a spectral resolution varying between 0.015 to 0.03 μm and has a flux accuracy of approximately 5 % throughout most of its spectral range.

2.2 Model and Model Input

To examine the consistency of the spectral and broadband fluxes observed aboard the Egrett and Twin Otter, simulated fluxes were computed for a synthesized cloud field using a 3-D Monte Carlo based radiative transfer model described in O'Hirok and Gautier (1998a). Two simulations were conducted. The first simulation uses best estimates of the optical properties of the atmosphere occurring at the time as input to the model (i.e. atmospheric gases, aerosols, cloud microphysics, surface albedo). The second simulation is a sensitivity study that uses optical properties adjusted to best match the observed fluxes.

The synthetic cloud field optical thickness is derived from regridding the 0.500 μm downwelling

flux (17:30 - 19:21 UTC) measured aboard the Twin Otter to 400 points and matching the irradiance at each point to plane-parallel cloud radiative transfer computations (Ricchiazzi et al., 1998) for similar cloud and atmospheric conditions. The mean cloud base and cloud top heights are estimated from the cloud detection lidar aboard the Egrett and a micropulse lidar located at the CART central facility. The cloud layer is partitioned vertically into 30 layers, each 40 meters thick. Horizontally, the layers are sectioned into cells of 1 km length over a distance of about 400 km. Cloud top altitude variability is related to the total liquid water path (LWP) of each horizontal column. The vertical distribution of cloud liquid water content varies with the slope of the adiabatic curve but at an amount representing less than 40% of the saturated adiabatic liquid water content. Internal variations of the LWC are based on a multiplicative cascade approach that uses weighting coefficients derived directly from the variability of the LWP (O'Hirok and Gautier, 1998b). Optical properties within each cell are homogeneous. The liquid water content (LWC) of a given cell is related to the extinction coefficient, σ_{ext}, by the expression

$$\sigma_{ext} = (3\, Q_{ext}\, LWC) / (4\, \rho\, r_e) \tag{1}$$

where r_e is the effective radius of the cloud droplet distribution, Q_{ext} is the cloud droplet extinction efficiency, and ρ is the density of water.

Although the radiative fluxes are highly sensitive to r_e, no direct measurements of this quantity are available. In this study, we took what we consider the most conservative approach and bounded r_e to values between 6 and 9 μm. The cloud droplet radius distribution is specified as a modified gamma size distribution. Within these limits, r_e is allowed to vary spatially according to the LWC (in g m^{-3}) at a specific location within the cloud layer and generally follows the relationship

$$r_e = 100 \times [\mathrm{LWC} \times 3 / (4\pi \times N)]^{1/3} \tag{2}$$

where N is the droplet number concentration taken as 600 cm^{-3} (Bower et al., 1994). Figure 1 shows cross-sections of LWC and r_e and the vertically integrated LWP for the synthetic cloud. The mean LWP is 316 g

m^{-2} equating to a mean optical thickness, τ, of 66 for an average r_e of 7.3 μm.

All model computations are performed at 0.005 μm spectral intervals from 0.25 to 5.00 μm using the three term *k*-distribution method of LOWTRAN7 (Kneizys et al. 1988). The cloud droplet single scattering albedo, extinction efficiency, and phase function are computed directly from Mie theory for each spectral interval (Wiscombe, 1980). As part of the sensitivity study, a second set of computations was performed and the cloud droplets' co-albedo multiplied by 3 to more closely match the observed absorptance for the TDDR channels at 1.501, 1.651 and 1.750 μm.

Model inputs of pressure, temperature, and water vapor vertical profiles are derived from the 17:30 UTC sounding at the CART site. These quantities are interpolated onto the model's 64 layer vertical grid, representing the atmosphere between the surface and 100 km. A standard ozone profile (McClatchey et al., 1972) is employed that has been adjusted to provide a total Dobson unit value (264) midway between those obtained at Boulder, Colorado and Nashville, Tennessee for 950130 (data obtained from the National Oceanic and Atmospheric Administration Climate Monitoring and Diagnostics Lab total ozone archive). For the strongest absorbing wavelengths, the results should be rather insensitive to the ozone profile since the altitude of the simulated fluxes is well below the altitude where the ozone concentration reaches its highest value.

For the surface, a Lambertian vegetation reflectance model is used to parameterize the shape of the spectral albedo (Reeves and Landen, 1975). To accurately portray the actual conditions during ARESE, this spectrum has been adjusted to provide a best fit to the observed TDDR spectral albedo without changing its overall shape. Additionally, the modeled albedo spectrum is constrained so that the broadband albedo is equal to the observed value of 0.17. Since the TDDR upwelling measurements aboard the Twin Otter are unreliable for 951030, the albedo observed from that aircraft for the clear-sky day of 951011 is used. While variations of surface albedo can dramatically alter the flux transmitted to the surface, the net effect on atmospheric absorption is negligible. Hence, errors in estimating the surface albedo should not alter any of the conclusions found in this study.

Aerosol represents a challenge for model input, since radiative fluxes in the visible region of the solar spectrum are highly sensitive to their concentration and microphysics. Although measurements of aerosol optical depth are routinely made for clear skies by directly looking at the sun, sun photometric

techniques cannot be employed for overcast conditions. Hence, the boundary layer aerosol optical depth must be estimated for 951030. Based on observations for clear days preceding 951030, we employ the same optical depth as used by Zender et al. (1997) of 0.12. Likewise, we use the same stratospheric aerosol optical depth of 0.006.

A rural type aerosol (Shettle and Fenn, 1975) represents the aerosol microphysics with the single scattering albedo set at 0.938 and the asymmetry factor specified at 0.67. These are based on climatological values as reported by d'Almeida et al. (1991). For the sensitivity study, the aerosol microphysics are altered so that the computed atmospheric absorptance at 0.500 μm equals the observed absorptance between the Egrett and the Otter. This adjustment represents an increase in aerosol optical depth to 0.17, a reduction in the aerosol single scattering albedo to 0.82, and a lowering of the asymmetry factor to 0.61. By increasing aerosol absorption, the albedo at the Egrett flight level is lowered. To bring the simulated albedo back to the observed for the sensitivity study, the cloud optical thickness is increased by 9%.

2.3 Model computations

Upwelling and downwelling irradiance were computed at all layers but stored for the Egrett flight level, Otter flight level, and surface. For simulating the broadband instruments, the results were spectrally integrated and convolved with the TSBR and FSBR supplied filter functions. An *a-priori* estimate of the photons required for the Monte Carlo computation is difficult to make. This difficulty arises because of the varying spectral nature of gaseous absorption, aerosols, surface albedo and cloud microphysics and the use of photon weights. Generally, for a given wavelength the termination of the Monte Carlo process is based on a convergence criterion as described in O'Hirok and Gautier (1998a). For non-TDDR wavelengths where broadband and spatial integration greatly reduces statistical noise, the Monte Carlo process is completed when the atmospheric absorption between the Egrett and ground, the upwelling irradiance at the Egrett, and the downwelling flux at the ground change by less than 0.5 % for each horizontal cell. For each of the TDDR wavelengths, the percent change was reduced to 0.1% in order to increase the number of photons and the accuracy of the computations. At each of these wavelengths at least 2,400,000 weighted photons were processed. Overall, at least 100 million weighted photons were utilized per cloud field simulation.

3 Results

In this section, we present a comparison between the modeled (using best estimates of atmospheric optical properties) and observed upwelling and downwelling fluxes and atmospheric absorption between the Egrett and Otter flight levels. It should be recalled that the cloud field used in the model computations is derived from the channel 1 (0.500 μm) downwelling flux measured aboard the Otter. Naturally, this condition will bias the fluxes such that better agreement will be found between modeled and observed downwelling fluxes below the cloud than for the upwelling fluxes at the Egrett flight level. However, since the atmospheric absorption is derived as the difference in the net fluxes modeled and observed at the two flight levels, there is no appreciable biases encounter in the computed absorption, and hence, there are no effects on the conclusions found in this study.

3.1 Broadband Upwelling and Downwelling Flux Flight Comparisons

First, we examine two quantities: the upwelling broadband radiation flux for the TSBR and FSBR instruments on the Egrett above the cloud system and the downwelling broadband radiation flux for the TSBR and FSBR instruments on the Otter below the cloud system. The results of our model computations are compared to the observations in Figures 2a and b, where the solid line represent the instantaneous flux and the dashed line the flight average. A large difference appears between the Egrett upwelling observations and model computations for the visible (VIS), near-infrared (NIR), and total broadband (TOTAL) spectral regions. However, for the zenith downwelling flux on the Otter, there is comparatively excellent agreement for the visible and a good agreement for the total but a significantly poorer agreement for the NIR. The excellent agreement with the VIS downwelling flux is to be expected since the cloud optical depth was derived from 0.500 μm TDDR downwelling irradiance measured aboard the Otter. Nonetheless, since the VIS is obtained as the difference between the TOTAL and the NIR, the agreement is not straightforward. This agreement in the VIS region and the disagreements in the two other spectral regions (TOTAL and NIR) suggest that if the two measurements (TOTAL and NIR) are biased, the biases cancel out. Also, proportionally, the bias for the zenith downwelling NIR flux would be larger than that for the TOTAL. Values representing these comparisons are presented in Table 1 (columns 1, 2 and 3).

3.2 TDDR Channels Flight Comparisons

As previously mentioned, in this paper we have modeled the TDDR spectral fluxes. Comparisons with the observations are presented in Figures 3a and b, and the results are quantified in Table 2a and b. For the zenith downwelling spectral flux, there is excellent agreement between the model fluxes and observations for all TDDR channels except channels 3 (1.064 μm) and 5 (1.501 μm). In the case of TDDR channel 5, the difference may be attributed to what seems to be a zero offset problem in the instrument. Since the cloud field was tuned to the Otter observed downwelling flux for channel 1 (0.500 μm) only, it was not fully expected that good agreement should also be found for channels 2, 4 and 6. Additionally, if there is absorption not fully accounted for in the model it is difficult to surmise an absorbing mechanism that would not partially reduce some of the downwelling flux in these channels. However, as noted previously, the downwelling flux below the cloud is highly sensitive to the surface albedo. Because vegetation is highly reflective in the near-infrared, relatively minor variations in the surface albedo estimate may mask reductions in transmittance through the cloud. Still, since absorption is computed from net fluxes and not just transmittance, errors in the estimate of surface albedo will have little impact on the calculation of atmospheric absorptance.

For the nadir upwelling spectral radiation flux at the Egrett (left panels), the results of the comparisons are generally poor for most channels except 0.862 μm, and generally deteriorate for the longer wavelength channels. The spatial smoothing of the 3-D computations for the upwelling flux is apparent in the good spatial coherence between the observed and modeled signals. Interestingly, the relationship inverts at the longest wavelengths, for which we cannot offer any explanation.

3.3 Flight-Averaged Albedo and Transmission Comparisons

To examine the consistency of the observed and modeled data, both spectrally and broadband, averages over the length of the flight and over the spectral interval covered by the instrument have been plotted in Figures 4a and b. The top figure (4a) shows the spectral variations of the flight-average modeled (thin line) albedo at the Egrett flight level, with the discrete spectral observations for the TDDR. Three of the SSP wavelengths for the Egrett flight level are also indicated on the figure. The bottom figure (4b) shows the spectral variations of the flight average model (thin line) transmission at the Otter flight level with the discrete spectral observations for the TDDR. On both figures the length of the vertical bars

indicate the magnitude of the standard deviation (from the flight average) of the model and observations during the flight. The broadband VIS, NIR and TOTAL values of albedo and transmission are also plotted next to each figure. As noted previously, the visible broadband is computed as the difference between the TSBR and FSBR for both model results and observations.

For albedo, the model results and the SSP observations are in exact agreement at 0.500 μm, suggesting the reasonableness of the model's computation and input. However, the TDDR's albedo at this wavelength is lower by about 0.05. Interestingly, the difference between the broadband VIS albedo and the model is much greater at 0.20. At 0.862 μm the SSP observed albedo falls between the modeled and the TDDR albedo. Further into the near-infrared, the difference for some of the spectral channels approaches 0.2 between the model and the TDDR and 0.12 for the broadband NIR. The largest discrepancy exists between the model computation and both the SSP and TDDR observed albedo at 1.064 μm. Overall, the broadband TOTAL observed albedo is .17 lower than the model results.

For transmission, with exception to the TDDR channel at 1.064 μm, there is excellent agreement (< .01) between the model results and observations. The observed transmission, lower by .03 for this channel, coincides with the large discrepancy in albedo, suggesting either a systematic instrument problem or a deficiency in model physics. The difference is even greater for the broadband NIR, where the observed transmission is .05 lower than the modeled.

3.4 SSP Spectral Comparisons

While the TDDR is limited to a single channel in the visible, the SSP on the Egrett provides continuous spectral data from 0.40 to 1.10 μm. Model computations of nadir upwelling spectral flux are compared to SSP observations of the same parameter in Figure 5 and presented in the form of band computations using a rectangular filter function in Table 3. General agreement exists between the SSP observations and the model computations at the 5% level. The largest differences occur near 0.76 μm and wavelengths further out in the near-infrared at 1.00 μm and higher. The first discrepancy is likely caused by the wide bandwidth of the SSP smoothing the strong molecular oxygen absorption feature at 0.76 μm. The latter, however, coincides with the albedo and transmission discrepancies found previously at 1.064 μm. For the SSP, part of the discrepancy above 1.00 μm may be related to the extreme sensitivity of typical silicon detectors to the temperature of the detector.

As previously noted, the SSP and model results match extremely well at 0.500 μm, and the difference between the model and TDDR albedo at this wavelength is less than .05. When integrated over the wavelengths from 0.42 and 0.68 μm the difference in albedo is less than .01 for the SSP and model, but it approaches .20 for the comparison between the broadband instruments and model computations. Thus, at least within the visible spectrum, the TDDR tends to be more consistent with the SSP and model results than with the broadband instruments. This result is consistent with the findings of Li et al. (1999).

3.6 Absorption Computations

Together, the comparisons presented above suggest that the model is fairly representative of the radiative environment that existed on 103095, and therefore it is reasonable to use it: 1) to interpolate between discrete measurements and 2) to compute the column spectral and broadband radiation absorption for that flight. Atmospheric absorption between the Egrett and Otter is computed by taking the difference between the net fluxes at the two flight levels. Since the upwelling flux measurements aboard the Twin Otter are unreliable for 951030, the upwelling flux at the Twin Otter level is computed by multiplying the Twin Otter level downwelling flux by the surface albedo. This method is used for both the observations and model computations to reduce any biases that may occur by neglecting the intervening atmosphere between the Twin Otter and the ground. In Figure 6, we show the modeled absorptance spectral variations of the flight-averaged atmospheric column (thin line) and compare these values with absorptance computed from the aircraft observations. The broadband results are shown to the right of the spectral plot. Again, the visible broadband is computed as the difference between the TOTAL and NIR broadband.

Significant differences exist between the computed and the observed absorptance, reflecting the differences in the albedo and transmission radiation discussed above. In general, the agreement is best for the shorter wavelengths regions (0.500 and 0.862 μm) and deteriorates for longer wavelengths. A large difference exists at 1.064 μm and at the two longest wavelength TDDR channels (1.651 and 1.750 μm). The differences between the broadband results are very large, about 135 Wm^{-2} for the total broadband. The overall broadband differences are presented in Table 1.

4 Enhanced Absorption Analysis

Temporarily ignoring the Egrett broadband measurements, the multiple data sets analyzed are still indicative of the possible existence of some degree of unexplained or "anomalous" absorption. The questions are then: 1) what is the magnitude of this unexplained absorption, and 2) what are the potential sources of this absorption. To address these questions we have attempted to modify the different input parameters to our model. This modification was made in such a way as to maximize the modeled absorption and reconcile the model results with the observations while keeping the input data within realistic bounds.

First we assume that it is reasonable, in a first evaluation, to exclude the cloud field representation as a source of uncertainty. This assumption is based on the general agreement between observations and model computations in the visible portion of the spectrum. (Note this assumption would not be valid if there exists an unaccounted for, spectrally flat absorber) Accordingly, the following input parameters can be modified in order to improve comparisons: 1) the atmospheric profiles of water vapor and ozone, 2) the surface albedo, and 3) aerosol and cloud droplet properties. A sensitivity study can easily show that unrealistic changes in water vapor and ozone amount would be necessary to reconcile model computations and observations. Although surface albedo changes can strongly modify the transmission to the surface under a cloudy sky, their effect on overall absorption is very small and, henceforth, ignored. On the other hand, changes in aerosol and cloud droplet properties can be altered in such a way as to definitely improve the comparisons.

The results of these modifications are presented in Figure 7. Changes in aerosol properties were made as described in section 2.2, whereas changes in cloud droplet properties were included in terms of a small increase in cloud optical depth (a factor of 1.09) and an increased in co-albedo by a factor of three. The increase in co-albedo forces higher absorption by cloud droplets without specifying the process that induces such an increase. As shown in Figure 7, the agreement with these tuned parameters is excellent for most of the TDDR channels. There remains some minor overestimation of absorption at 1.249 and 1.501 μm. However, those differences are small compared to the large discrepancy remaining at 1.064 μm, where the absorption by the model is still much smaller than that observed.

The right hand area of Figure 7 presents a comparison between broadband (VIS, NIR and TOTAL)

computations and observations. Despite the significant changes in aerosol and cloud microphysical properties, this comparison still indicates a large disagreement between model computations and observations. The total difference has been reduced to about 97 Wm^{-2} . This reduced discrepancy is still inconsistent, however, with the relative agreement now obtained with the spectral observations.

If we analyze in detail the amount of enhanced absorption that each of the changes produce, we find that the aerosol changes induced about 20 Wm^{-2}, and the co-albedo increase resulted in about the same amount, or 20 Wm^{-2}. Still, a discrepancy at (and likely around) 1.064 μm exists in both the TDDR and the SSP data. We now attempt to evaluate the maximum potential contribution to the broadband absorption of this unexplained absorption in that spectral region. We use the data to guide us, while making a number of assumptions. The SSP suggests that the absorption anomaly has a broad feature. We can maximize this feature's contribution by assuming that: 1) its spectral extent is from 0.96 to 1.2 μm (overlapping with the water vapor absorption) and 2) there is as much absorption observed in transmission as there is observed in albedo by the SSP. Centered about this feature at 1.064 μm, the net effect is an additional 20 –25 Wm^{-2} enhanced absorption.

Considering the relatively good agreement between the model and the spectral observations after adjustment of the input parameters and the maximization of absorption centered around 1.064 μm, there still remains a discrepancy of about 75 – 80 Wm^{-2} for the broadband absorption. These results suggest that either large absorption features exist between the spectral channels of the TDDR and are not accounted for in our model, or the spectral measurements are problematic, or the Egrett upwelling broadband data (TSBR and FSBR) are in error. Considering the extreme care and thoroughness that have been applied to the radiometric, angular and spectral calibration of these instruments, it is difficult to speculate on the source of that error.

5 Discussion

One of the main controversies surrounding the anomalous absorption topic, besides its very existence, is whether its magnitude requires the introduction of new physics into climate models. Our results have shown that even if we treat the broadband measurements as problematic, several puzzling questions still remain. The first concerns interstitial aerosols. The values for the single scattering albedo

(0.82) and the asymmetry factor (0.61) that are required to match the observations are much lower than those expected for typical rural aerosols. They are not totally unrealistic, however, if one considers the possibility of large aerosol particles, which have a strong forward scattering coefficient and large absorption properties. Also, these results are consistent with those obtained in clear sky conditions for which the reconciliation of diffuse component observations and model computations require similar changes in aerosol microphysics (Kato et al., 1997, Ricchiazzi et al., 1999).

Next, a cloud water droplet co-albedo of 3 times that predicted by Mie scattering for pure water droplets is required to bring model calculations in line with observations. This result is in keeping with that found by other investigators analyzing cloud reflectance spectra (Twomey and Cocks, 1982; Stephens and Platt, 1987). The presence of absorbing material such as soot inside the water droplets can dramatically increase the co-albedo of a cloud droplet (Chýlek et al., 1984). Using a Mie scattering code (Wiscombe, 1980) we determined that a cloud droplet containing a soot particle of 0.5 μm at its core raises the co-albedo by approximately a factor of 3 for the TDDR channels of 1.501, 1.651 and 1.750 μm. For an estimate of the radiative effects of this cloud droplet for a cloud similar to the 103095 case we used a plane-parallel based radiative transfer model (SBDART, Ricchiazzi et al., 1998). As shown in Table 4, the new computed absorptance values for the TDDR channels of 1.501, 1.651 and 1.750 μm are close to observed. However, at the shorter wavelengths the absorptance is unrealistically high, with values many times those observed. From these computations it is clear that the inclusion of a soot core within a cloud droplet does not offer a satisfactory explanation to the absorption anomaly.

Equally intriguing as the co-albedo problem is the unexplained absorption at 1.064 μm. Although this spectral region is basically devoid of major absorbers (except water vapor at 1.1 μm), it does contain O_2-O_2 dimers. While the reported absorption cross-section of these dimers is not large enough to explain such a large absorption, it is possible that unknown dimer-related processes are at work. To investigate this issue we have included the most recent absorption cross-section as reported by Solomon (personal communication) in SBDART. With this new cross section the optical depth is of the order of 0.015. The result is an increase in cloudy column absorption of only 0.49 Wm^{-2}. Clearly, the effects of adding the new O_2-O_2 cross section are not sufficient to explain the discrepancy between model computations and observations by both the SSP and the TDDR.

6. Conclusions

We have presented comparisons between modeled and observed radiative flux in the broadband and spectral domains, and we have shown that a significant discrepancy exists between modeled and observed broadband fluxes. This difference is much greater than that expected from the reported uncertainties attributed to either radiometric and angular calibration of the instruments or the uncertainty in model input. We performed a consistency analysis using the spectral observations and the model to integrate for wavelengths between the spectral observations. Even after modifying the model inputs and microphysics and maximizing the absorption in the vicinity of 1.06 μm, the difference in total broadband absorption is still of the order of 75 Wm^{-2}. These results show that either there exist large undefined absorbers in the wavelengths between the TDDR channels, or more likely, the broadband observations are problematic as suggested by Li et al. (1999).

Nevertheless, focusing on the spectral observations alone, our analysis suggests that there is some unexplained absorption in the cloudy atmosphere of day 951030 over the CART site in Oklahoma. Both the aerosol and cloud microphysical absorption properties need to be enhanced to reproduce the observations. One could speculate that both aerosols and cloud properties are loaded with soot containing particles that absorb in an unusual manner, but preliminary radiative transfer computations suggest that the spectral signature of absorption for water droplets containing soot cores would be quite different from that observed. A puzzle perhaps more difficult to reconcile is that no known effect can be included in the model simulations to increase absorption to the values observed by both the TDDR and the SSP in the vicinity of 1.064 μm.

This study suggests the need for additional co-located broadband and spectral observations in clear and cloudy sky conditions over different regions of the world. In-situ aerosol and cloud droplet microphysical measurements would be important to unravel the role of these particles in the "anomalous absorption" topic. The need for such research efforts is not new. It has been almost two decades since Twomey and Cocks (1982) reported that to match observed cloud reflectance with theory in the near-infrared the co-albedo of cloud droplets needed to be increased by a factor of three- to five, an enhancement not far from that found in this study.

Acknowledgments. We wish to thank Francisco Valero, Graeme Stephens, Brett Bush and Reneta McCoy for providing the aircraft observation data. Helpful comments from two anonymous reviewers were greatly appreciated. This work was funded from the Department of Energy Grants 90ER61062 and 90ER61986.

References

Bower, K. N., T. W. Choularton, J. Latham, J. Nelson, M. B. Baker, and J. Jensen, A parameterization of warm clouds for use in atmospheric general circulation models. *J. Atmos. Sci., 51*, 2722-2732, 1994.

Cess, R. D. and co-authors, Absorption of solar radiation by clouds: Observations versus models, *Science, 267*, 496-499, 1995.

Cess, R. D., M. H. Zhang, Y. Zhou, X. Jing, and V. Dvortsov, Absorption of solar radiation by clouds: Interpretations of satellite, surface and aircraft measurements, *J. Geophys. Res., 101*, 23299-23309, 1996

Chýlek, P. V. Ramaswamy and R. J. Cheng, Effect of graphitic carbon on the cloud albedo of clouds, *J. Atmos. Sci., 41*, 3076-3084, 1984.

Collins, W. D., A global signature of enhanced shortwave absorption by clouds, *J. Geophys. Res., 103*, 31,669-31,679, 1998.

D'Almeida, G. A., P. Koepke and E. P. Shettle, Atmospheric aerosols: Global climatology and radiative characteristics, A. Deepak, Hampton, Va., 561 pp., 1991.

Imre, D. G., E. H. Abramson, and P. H. Daum, Quantifying cloud-induced shortwave absorption: An examination of uncertainties and of recent arguments for large excess absorption, *J. Appl. Meteor, 35*, 1991-2010, 1996.

Kato, S., T. P. Ackerman, E. E. Clothiaux, J. H. Mather, and others, Uncertainties in modeled and measured clear-sky surface shortwave irradiances, *J. Geophys. Res., 102*, 25881-25898, 1997.

Kneizys, F. X., E. P. Shettle, L. W. Abreeu, J. H. Chetwind, G. P. Anderson, W. O. Allery, J. E. A. Selby, and S. A. Clough, AFGL-TR-88-0177, Phillips Lab., Hanscom AFB, MA, 137 pp. [NTIS 206733], 1988

Li, Z., and L. Moreau, Alteration of atmospheric solar radiation by clouds: Simulation and observation, *J. Appl. Meteorol., 35,* 653-670, 1996.

Li, Z., A. P. Trishchenko, H. W. Barker, G. L. Stephens, and P. Partain, Analyses of Atmospheric Radiation Measurement (ARM) program's Enhanced Shortwave Experiment (ARESE) multiple data sets for studying cloud absorption, *J. Geophys. Res., 104,* 19,127-19134, 1999.

McClatchey, R. A., R.W. Fenn, J. E.A. Selby, F.E.Volz, and J. S. Garing, Optical properties of the atmosphere, *Tech Rep. Environ. Res. Pap., 411*, Air Force Cambridge Res. Lab., Bedford, Mass., 1972.

O'Hirok, W., and C. Gautier, A three-dimensional radiative transfer model to investigate the solar radiation within a cloudy atmosphere. Part I: Spatial effects. *J. Atmos. Sci., 55*, 2162-2179, 1998a.

O'Hirok, W., and C. Gautier, Comparison of GCM column shortwave radiative fluxes with three-dimensional simulated observations, *Proceedings of the Eighth Atmospheric Radiation Measurement (ARM) Science Team Meeting,* pp. 541-544, United States Department of Energy, Washington D. C., 1998b

Pilewskie, P., and F. P. J. Valero, Direct observations of excess solar absorption by clouds, *Science, 267,* 1626-1629, 1995.

Ramanathan, V., The role of earth radiation budget studies in climate and general circulation research, *J.*

Geophys. Res., 92, 4075-4095, 1987.

Ramanathan, V., B. Subasilar, G. Zhang, W. Conant, R. Cess, J. Kiehl, H. Grassl, and L. Shi, Warm pool heat budget and shortwave cloud forcing: A missing physics. *Science, 267,* 499-503, 1995.

Reeves, R.G., A. Anson, and D. Landen, Eds., Manual of remote sensing, American Society of Photogrammetry, 1st ed. Falls Curch, Va., 1975.

Ricchiazzi, P., S. Yang, C. Gautier, and D. Sowle, SBDART: A research and teaching tool for plane-parallel radiative transfer in the Earth's atmosphere, *Bull. Am. Meteorol. Soc., 79,* 2101-2114, 1998.

Ricchiazzi, P., C. Gautier, and T. Tooman, Aerosol properties from surface radiation observations, in *Proceedings of the ninth Atmospheric Radiation Measurement (ARM) Science Team Meeting,* in press, United States Department of Energy, Washington D. C., 1999

Shettle, E. P., and R. W. Fenn, Model of the atmospheric aerosols and their optical properties, in *AGARD conference proceedings no. 183,* pp. 2.1-2.16, AGARD, Neuilly sur Seine, France, 1975.

Stephens, G. L., and S.-C. Tsay, On the cloud absorption anomaly, *Q. J. R. Meteorol. Soc., 116,* 671-704, 1990.

Stephens, G. L. and C. M. R. Platt, Aircraft observations of the radiative and microphysical properties of stratocumulus and cloud fields, *J. Climate Appl. Meteor., 26,* 1243-1269, 1987.

Twomey, S. and T. Cocks, Spectral Reflectance of clouds in the near-infrared: Comparisons of measurements and calculations, *J. Meteor. Soc. Japan*, 60, 583-592, 1982

Valero, F. P. J., R. D. Cess, M. Zhang, S. K. Pope, A. Bucholtz, B. Bush and J. Vitko Jr., Absorption of solar radiation by the cloudy atmosphere: Interpretations or collocated aircraft measurements, *J. Geophys. Res., 102,* 29917-29927, 1997a.

Valero, F. P. J., A. Bucholtz, B. Bush, S. K. Pope, W. D. Collins, P. Flatau, A. Strawa and W. J. Y. Gore, Atmospheric radiation Measurements Enhanced Shortwave Experiment (ARESE): Experimental and data details, *J. Geophys. Res., 102,* 29929-29937, 1997b.

Waliser, D. E., W. D. Collins, and S. P. Anderson, An estimate of the surface shortwave cloud forcing over the western Pacific during TOGA COARE, *Geophys. Res. Lett., 23,* 519-522, 1996.

Wiscombe, W. J., Improved Mie scattering algorithms, *Appl. Opt., 19,* 1505-1509, 1980.

Zender, C. S., B. Bush, S. Pope, A. Bucholtz, W. D. Collins, J. T. Kiehl, F. P. Valero and J. Vitko Jr, Atmospheric absorption during the Atmospheric Radiation Measurement (ARM) Enhanced Shortwave Experiment (ARESE), *J. Geophys. Res., 102,* 29901-29915, 1997.

Figure Captions

Fig. 1(a) Synthetic cloud liquid water concentration (1b) and effective radius cross-sections. (1c) Synthetic cloud vertically integrated liquid water path.

Fig. 2(a) Egrett flight level observed (dark) and modeled (light) broadband visible, near-infrared and total upwelling solar irradiance. 2(b) Same as Figure 2a but for Otter flight level downwelling solar irradiance. Dashed lines represent mean values for observed and modeled fluxes averaged over the 400 km flight path.

Fig. 3(a) Egrett flight level observed (dark) and modeled (light) TDDR channels of 0.500, 0.862, 1.064, 1.249, 1.501, 1.651 and 1.750 μm upwelling solar irradiance. 3(b) Same as Figure 3a but for Otter flight level downwelling solar irradiance. Dashed lines represent mean values for observed and modeled fluxes averaged over the 400 km flight path.

Fig. 4(a) Egrett flight level modeled spectral albedo average along flight path (gray line). Modeled (+) and observed (*) albedo average and standard deviation of flight path at TDDR channels of 0.500, 0.862, 1.064, 1.249, 1.501, 1.651 and 1.750 μm. (diamond) SSP albedo average and standard deviation of flight path at TDDR channels of 0.500, 0.862 and 1.064. 4(b) Egrett flight level observed (dark) and modeled (light) broadband visible, near-infrared and total albedo. 4(c) Same as Figure 4a, but for Otter flight level transmission and without SSP measurements. 4(d) Same as Figure 4b, but for Otter flight level transmission.

Fig. 5 Average spectral upwelling solar irradiance at Egrett flight level for SSP (dark) and model (light). The modeled flux has been smooth by a 25 nm moving average to better match the effects of the SSP bandwidth.

Fig. 6(a) Modeled average spectral atmospheric absorptance between Egrett and Otter (gray line). Modeled (+) and observed (*) average and standard deviation atmospheric absorptance between Egrett and Otter along flight path at TDDR channels of 0.500, 0.862, 1.064, 1.249, 1.501, 1.651 and 1.750 μm. 6(b) Egrett flight level observed (dark) and modeled (light) broadband visible, near-infrared and total absorptance between Egrett and Otter.

Fig. 7(a) Same as Figure 6a, but for adjusted cloud droplet co-albedo and aerosol. 7(b) Same as Figure 6b, but for adjusted cloud droplet co-albedo and aerosol.

Table Legends

Table 1 Broadband visible, broadband near-infrared and broadband total Egrett nadir, Otter zenith and absorbed solar radiation between aircraft. Values are for observed, modeled (1), observed – modeled (1), adjusted co-albedo and aerosol modeled (2), observed – modeled (2). Modeled (2) values represent the adjustment in aerosol and cloud droplet optical properties.

Table 2 TDDR channels (a) Egrett nadir and (b) Otter zenith fluxes. Values are for observed, modeled (1), observed – modeled (1), adjusted co-albedo and aerosol modeled (2), observed – modeled (2).

Table 3 SSP integrated upwelling irradiance. Values are for observed, modeled (1), observed – modeled (1), adjusted co-albedo and aerosol modeled (2), observed – modeled (2).

Table 4 TTDR channels atmospheric absorptance. Values are for observed, modeled pure water droplet, water droplet co-albedo x 3, and water droplet with 0.5 um soot core. Model results are based on SBDART computations.

Table 1

	observed Wm^{-2}	modeled 1 Wm^{-2}	differ. 1 Wm^{-2}	modeled 2 Wm^{-2}	differ. 2 Wm^{-2}
BB VIS					
Egrett Nadir	214.0	317.6	-103.6	307.0	-93.0
Otter Zenith	55.3	53.8	1.5	50.7	4.6
Absorbed	79.7	13.0	66.7	26.4	53.2
BB NIR					
Egrett Nadir	234.7	282.8	-48.1	260.6	-25.9
Otter Zenith	25.1	45.3	-20.2	38.8	-13.7
Absorbed	220.0	149.2	70.8	175.8	44.2
BB TOTAL					
Egrett Nadir	448.7	600.4	-151.7	567.7	-118.9
Otter Zenith	81.4	99.1	-17.7	89.5	-8.1
Absorbed	299.7	162.2	137.5	202.2	97.4

Table 1 Broadband visible, broadband near-infrared and broadband total Egrett nadir, Otter zenith and absorbed solar radiation between aircraft. Values are for observed, modeled (1), observed – modeled (1), adjusted co-albedo and aerosol modeled (2), observed – modeled (2). Modeled (2) values represent the adjustment in aerosol and cloud droplet optical properties

Table 2a

Egrett Nadir Up	**observed** $Wm^{-2}\mu m^{-1}$	**modeled 1** $Wm^{-2}\mu m^{-1}$	**differ. 1** $Wm^{-2}\mu m^{-1}$	**modeled 2** $Wm^{-2}\mu m^{-1}$	**differ. 2** $Wm^{-2}\mu m^{-1}$
TDDR Ch 1 (0.500)	970.6	1056.7	-86.1	1022.3	-51.7
TDDR Ch 2 (0.862)	506.7	539.8	-33.1	526.2	-19.5
TDDR Ch 3 (1.064)	292.6	353.2	-60.6	340.6	-48.0
TDDR Ch 4 (1.249)	219.0	234.6	-15.6	210.2	8.8
TDDR Ch 5 (1.501)	49.8	74.6	-24.8	47.6	2.2
TDDR Ch 6 (1.651)	76.4	99.0	-22.6	77.1	-0.7
TDDR Ch 7 (1.750)	55.9	68.7	-12.8	52.2	3.7

Table 2b

Otter Zenith Down	**observed** $Wm^{-2}\mu m^{-1}$	**modeled 1** $Wm^{-2}\mu m^{-1}$	**differ. 1** $Wm^{-2}\mu m^{-1}$	**modeled 2** $Wm^{-2}\mu m^{-1}$	**differ. 2** $Wm^{-2}\mu m^{-1}$
TDDR Ch 1 (0.500)	178.7	185.2	-6.5	174.4	4.3
TDDR Ch 2 (0.862)	104.0	104.0	0.0	96.9	7.1
TDDR Ch 3 (1.064)	61.4	69.4	-8.0	61.2	0.2
TDDR Ch 4 (1.249)	36.6	36.8	-0.2	25.0	11.6
TDDR Ch 5 (1.501)	4.5	3.5	1.0	1.0	3.5
TDDR Ch 6 (1.651)	8.5	8.4	0.1	3.8	4.7
TDDR Ch 7 (1.750)	4.9	5.0	-0.1	2.1	2.8

Table 2 TDDR channels (a) Egrett nadir and (b) Otter zenith fluxes. Values are for observed, modeled (1), observed – modeled (1), adjusted co-albedo and aerosol modeled (2), observed – modeled (2).

Table 3

SSP	observed Wm-2	modeled 1 Wm-2	differ. 1 Wm-2	modeled 2 Wm-2	differ. 2 Wm-2
Band 1 (0.420 – 0.680 μm)	249.1	252.0	-2.9	241.8	7.3
Band 2 (0.685 – 0.940 μm)	135.0	141	-6.0	136.6	-1.6
Band 3 (0.945 – 1.100 μm)	40.7	53.0	-12.3	50.5	-9.9
Total	424.8	445.9	-21.2	428.9	-4.2

Table 3 SSP integrated upwelling irradiance. Values are for observed, modeled (1), observed – modeled (1), adjusted co-albedo and aerosol modeled (2), observed – modeled (2).

Table 4

Absorptance	**observed**	**pure water**	**co-albedo x 3**	**0.5 μm soot core**
TDDR Ch 1 (0.500)	0.039	0.013	0.013	0.350
TDDR Ch 2 (0.862)	0.053	0.013	0.024	0.370
TDDR Ch 3 (1.064)	0.217	0.063	0.093	0.388
TDDR Ch 4 (1.249)	0.170	0.156	0.252	0.413
TDDR Ch 5 (1.501)	0.705	0.572	0.730	0.634
TDDR Ch 6 (1.651)	0.445	0.310	0.480	0.450
TDDR Ch 7 (1.750)	0.534	0.404	0.558	0.520

Table 4 TTDR channels atmospheric absorptance. Values are for observed, modeled pure water droplet, water droplet co-albedo x 3, and water droplet with 0.5 um soot core. Model results are based on SBDART computations.

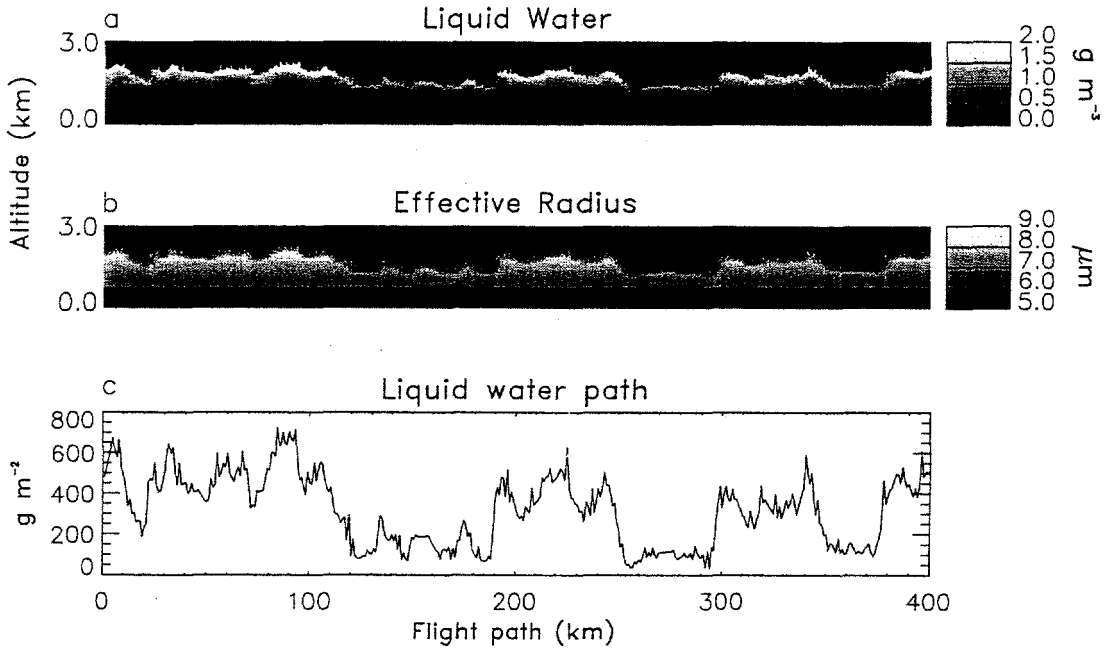

Fig. 1(a) Synthetic cloud liquid water concentration (1b) and effective radius cross-sections. (1c) Synthetic cloud vertically integrated liquid water path.

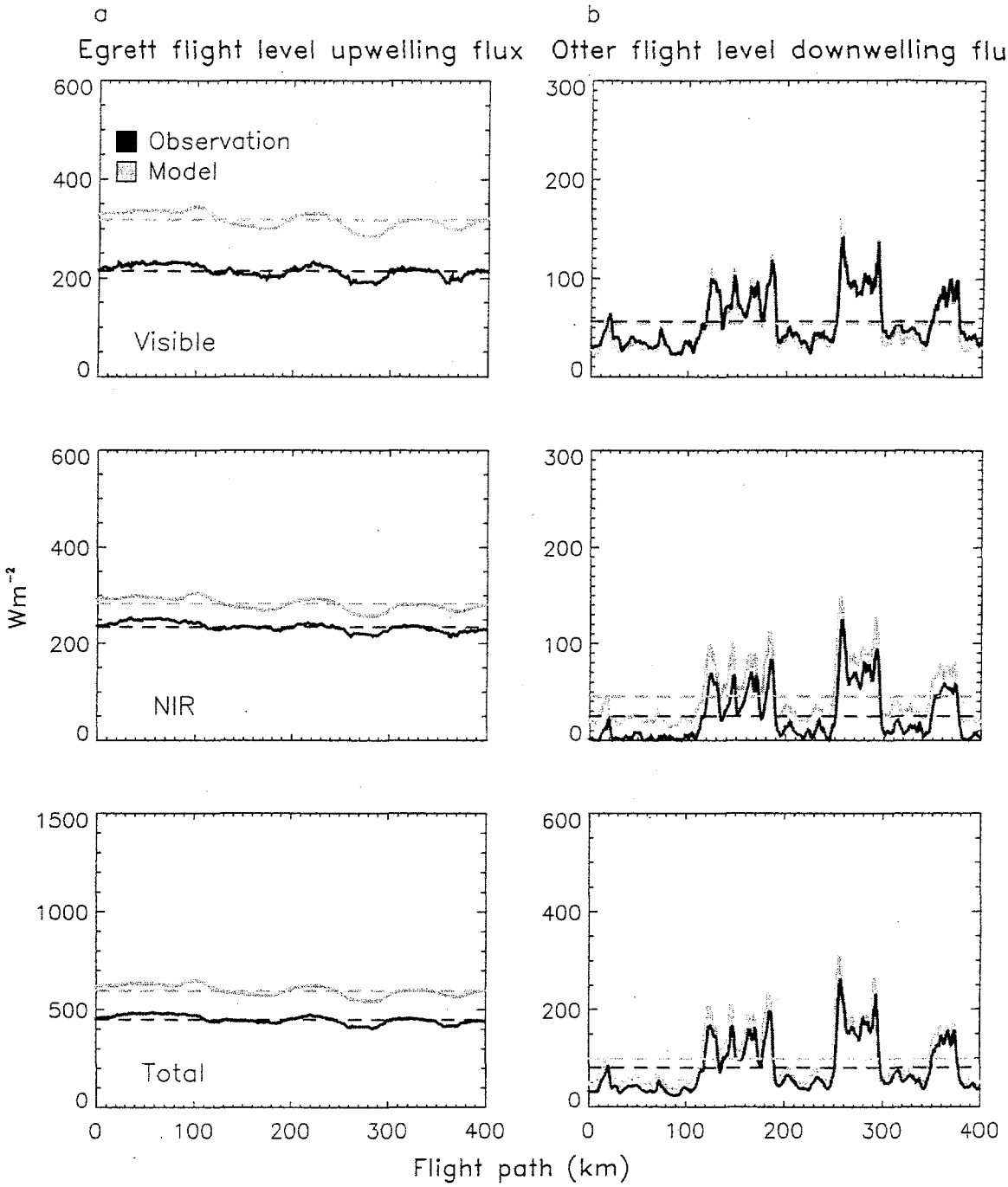

Fig. 2(a) Egrett flight level observed (dark) and modeled (light) broadband visible, near-infrared and total upwelling solar irradiance. 2(b) Same as Figure 2a but for Otter flight level downwelling solar irradiance. Dashed lines represent mean values for observed and modeled fluxes averaged over the 400 km flight path.

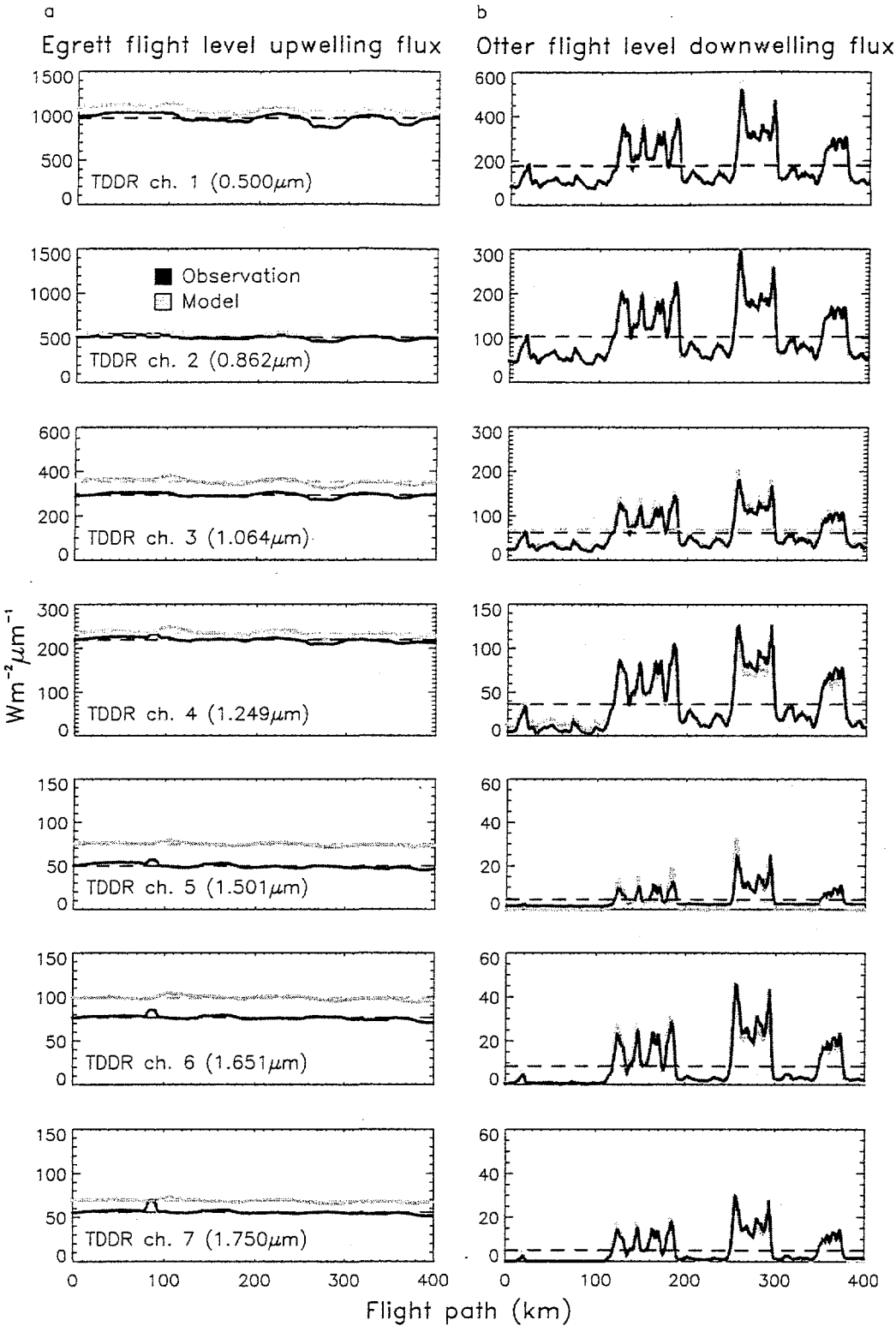

Fig. 3(a) Egrett flight level observed (dark) and modeled (light) TDDR channels of 0.500, 0.862, 1.064, 1.249, 1.501, 1.651 and 1.750 μm upwelling solar irradiance. 3(b) Same as Figure 3a but for Otter flight level downwelling solar irradiance. Dashed lines represent mean values for observed and modeled fluxes averaged over the 400 km flight path.

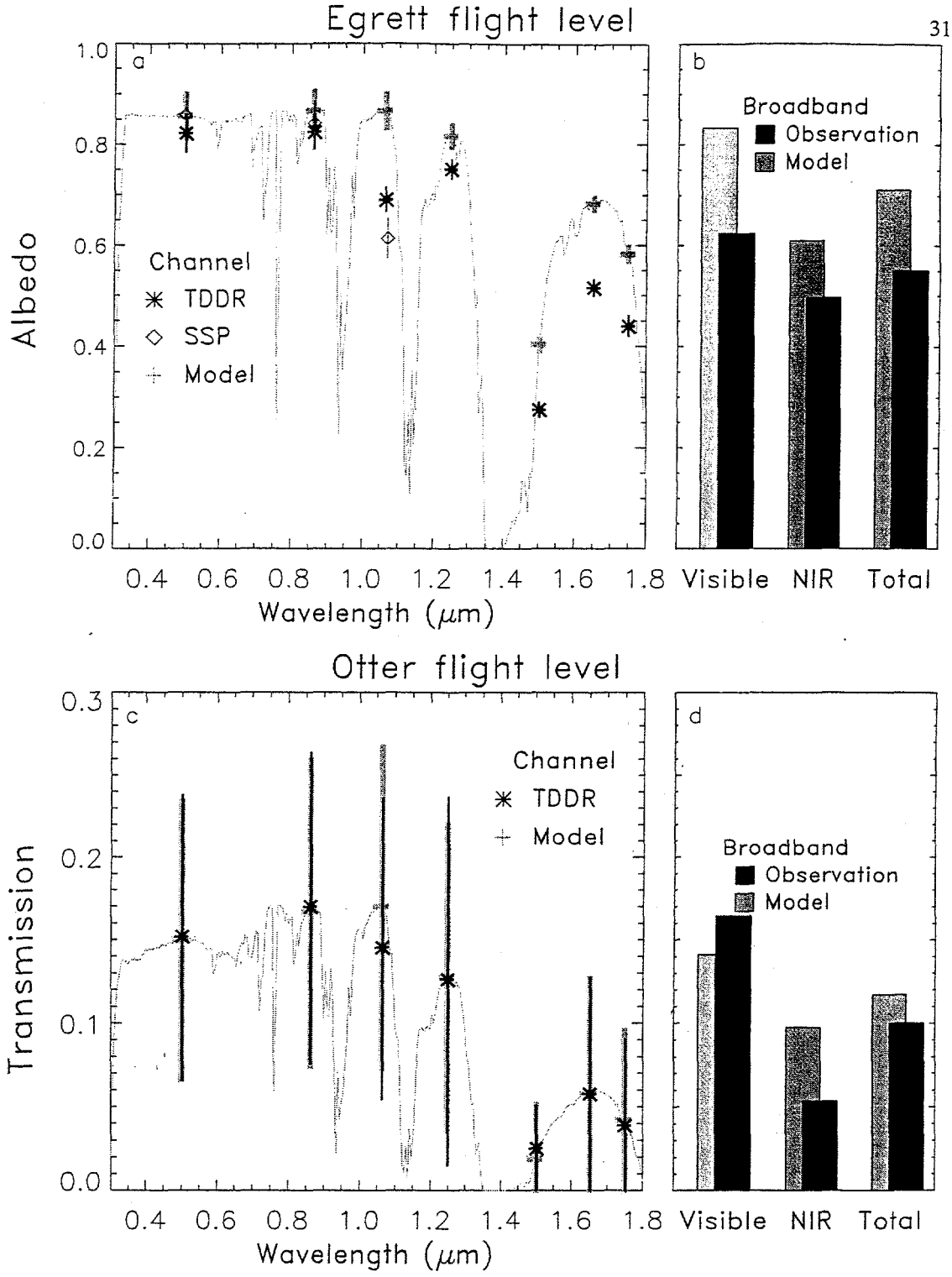

Fig. 4(a) Egrett flight level modeled spectral albedo average along flight path (gray line). Modeled (+) and observed (*) albedo average and standard deviation of flight path at TDDR channels of 0.500, 0.862, 1.064, 1.249, 1.501, 1.651 and 1.750 μm. (diamond) SSP albedo average and standard deviation of flight path at TDDR channels of 0.500, 0.862 and 1.064. 4(b) Egrett flight level observed (dark) and modeled (light) broadband visible, near-infrared and total albedo. 4(c) Same as Figure 4a, but for Otter flight level transmission and without SSP measurements. 4(d) Same as Figure 4b, but for Otter flight level transmission.

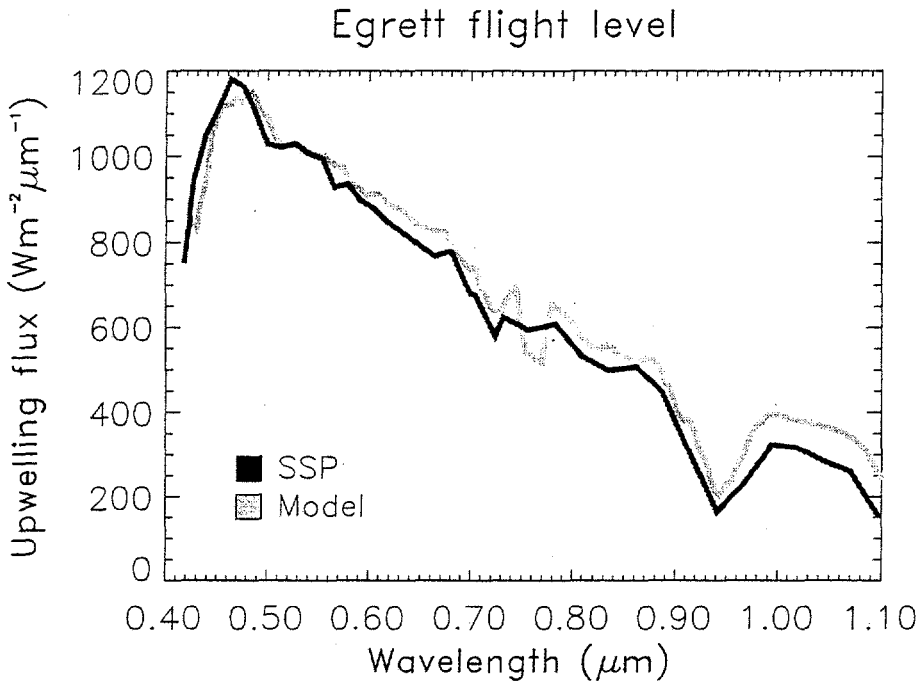

Fig. 5 Average spectral upwelling solar irradiance at Egrett flight level for SSP (dark) and model (light). The modeled flux has been smooth by a 25 nm moving average to better match the effects of the SSP bandwidth.

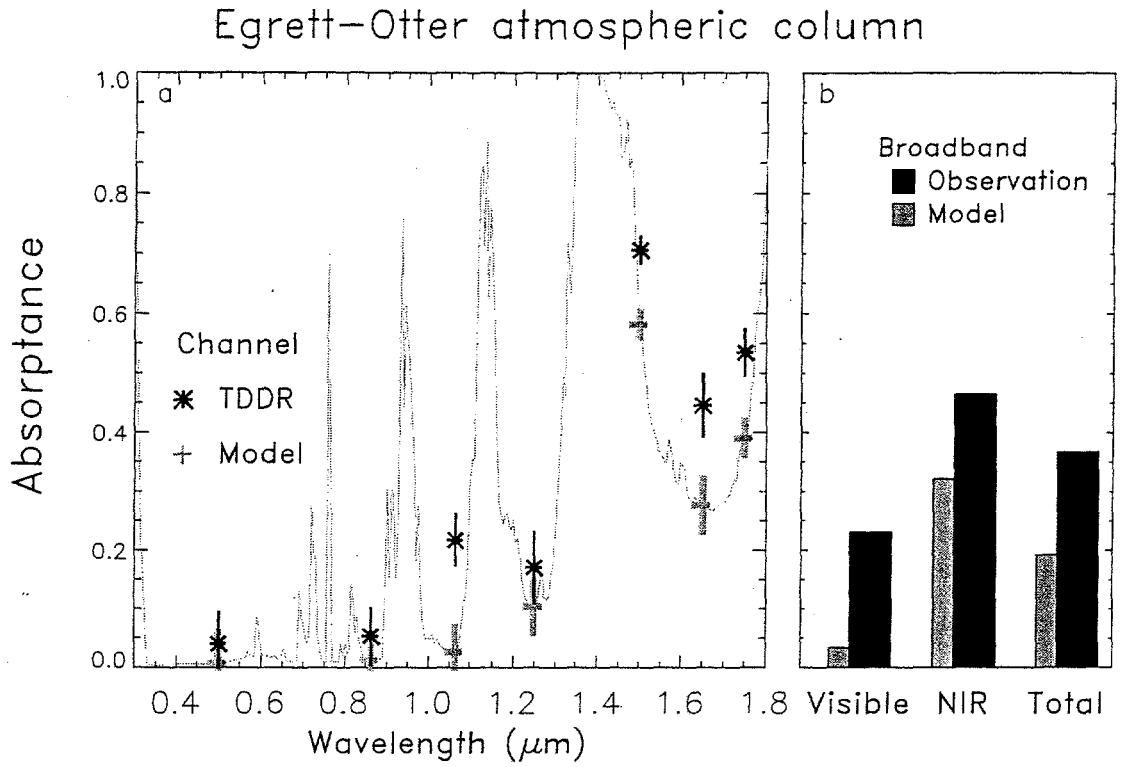

Fig. 6(a) Modeled average spectral atmospheric absorptance between Egrett and Otter (gray line). Modeled (+) and observed (*) average and standard deviation atmospheric absorptance between Egrett and Otter along flight path at TDDR channels of 0.500, 0.862, 1.064, 1.249, 1.501, 1.651 and 1.750 μm. 6(b) Egrett flight level observed (dark) and modeled (light) broadband visible, near-infrared and total absorptance between Egrett and Otter.

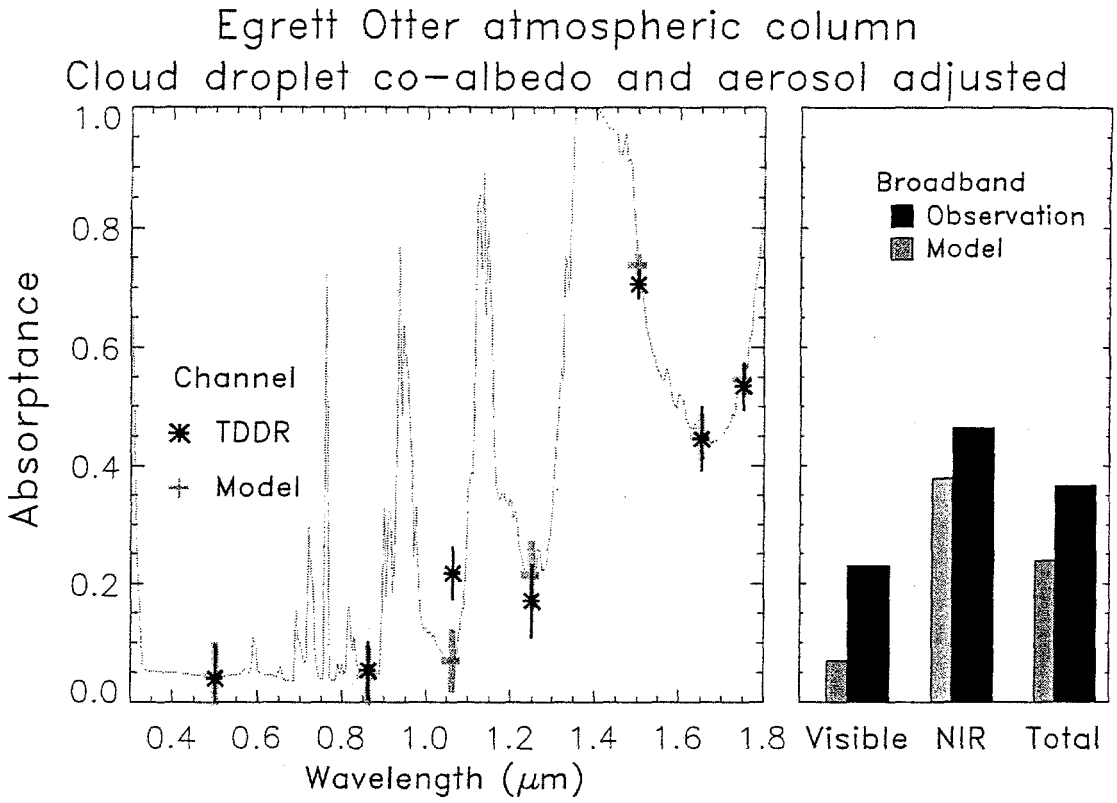

Fig. 7(a) Same as Figure 6a, but for adjusted cloud droplet co-albedo and aerosol. 7(b) Same as Figure 6b, but for adjusted cloud droplet co-albedo and aerosol.